HHS Public Access

Author manuscript

Cancer Res. Author manuscript; available in PMC 2022 July 14.

Published in final edited form as:

Cancer Res. 2021 April 01; 81(7): 1896–1908. doi:10.1158/0008-5472.CAN-20-1641.

MYCN-amplified neuroblastoma is addicted to iron and vulnerable to inhibition of the system Xc-/glutathione axis

Konstantinos V. Floros[1,*], **JinYang Cai**[1,*], **Sheeba Jacob**[1,*], **Richard Kurupi**[1], **Carter K. Fairchild**[1], **Mayuri Shende**[2], **Colin M. Coon**[1], **Krista M. Powell**[1], **Benjamin R. Belvin**[1,3], **Bin Hu**[2], **Madhavi Puchalapalli**[2], **Sivapriya Ramamoorthy**[4], **Kimberly Swift**[4], **Janina P. Lewis**[1,3,5], **Mikhail G. Dozmorov**[6], **John Glod**[7], **Jennifer E. Koblinski**[2], **Sosipatros A. Boikos**[8], **Anthony C. Faber**[1,#]

[1]VCU Philips Institute, School of Dentistry and Massey Cancer Center, Richmond VA, 23298 USA.

[2]Department of Pathology, Virginia Commonwealth University and Massey Cancer Center, Richmond VA, 23298 USA.

[3]Department of Biochemistry, Virginia Commonwealth University, Richmond VA, 23298 USA.

[4]Discovery and Translational Sciences, Metabolon Inc., Research Triangle NC, 27560 USA.

[5]Department of Microbiology and Immunology, Virginia Commonwealth University, Richmond VA, 23298 USA.

[6]Department of Biostatistics, Virginia Commonwealth University, Richmond VA, 23298 USA.

[7]National Cancer Institute Pediatric Oncology Branch, Bethesda MD, 20892 USA.

[8]Division of Hematology, Oncology and Palliative Care, Virginia Commonwealth University and Massey Cancer Center, Richmond VA, 23298 USA.

Abstract

MYCN is amplified in 20–25% of neuroblastoma, and MYCN-amplified neuroblastoma contributes to a large percent of pediatric cancer-related deaths. Therapy improvements for this subtype of cancer is a high priority. Here we uncover a MYCN-dependent therapeutic vulnerability in neuroblastoma. Namely, amplified MYCN rewired the cell through expression

[#] **Corresponding author:** Dr. Anthony C. Faber, Address: Philips Institute for Oral Health Research VCU School of Dentistry and Massey Cancer Center, Perkinson Building Room 4134, 1101 East Leigh Street, P.O. Box 980566, Richmond VA 23298-0566, Telephone: 804-828-0841. acfaber@vcu.edu.

[*]equal contribution

Authors' Contributions

K.V. Floros: Conception and design, Development of methodology, Acquisition of data, Analysis and interpretation of data, Writing and/or revision of the manuscript, **JY. Cai**: Acquisition of data, **S. Jacob**: Acquisition of data**, R. Kurupi**: Acquisition of data, **C.K. Fairchild:** Acquisition of data, **M. Shende**: Acquisition of data, **C.M. Coon**: Acquisition of data, **K.M. Powell**: Acquisition of data, **B.R. Belvin**: Acquisition of data, **B. Hu**: Acquisition of data, **M. Puchalapalli**: Acquisition of data, **S. Ramamoorthy**: Development of methodology, **K. Swift**: Development of methodology, **J.P. Lewis**: Development of methodology, **M.G. Dozmorov**: Acquisition of data, Analysis and interpretation of data**, J. Glod:** Development of methodology**, J.E. Koblinski**: Development of methodology, Analysis and interpretation of data**, S.A. Boikos**: Analysis and interpretation of data**, A.C. Faber**: Conception and design, Development of methodology, Acquisition of data, Analysis and interpretation of data, Writing and/or revision of the manuscript.

Conflict of interest: A.C. Faber has served as a paid consultant for AbbVie. KS and PR are employees of Metabolon, Inc.

of key receptors, ultimately enhancing iron influx through increased expression of the iron import transferrin receptor 1 (TfR1). Accumulating iron caused reactive oxygen species (ROS) production, and MYCN-amplified neuroblastomas showed enhanced reliance on the system Xc- cystine/glutamate antiporter for ROS detoxification through increased transcription of this receptor. This dependence created a marked vulnerability to targeting the system Xc-/glutathione (GSH) pathway with ferroptosis inducers. This reliance can be exploited through therapy with FDA-approved rheumatoid arthritis (RA) drugs sulfasalazine (SAS) and auranofin: in MYCN-amplified, patient-derived xenograft models, both therapies blocked growth and induced ferroptosis. SAS and auranofin activity was largely mitigated by the ferroptosis inhibitor ferrostatin-1, antioxidants like NAC, or by the iron scavenger deferoxamine (DFO). DFO reduced auranofin-induced ROS, further linking increased iron capture in MYCN-amplified NB to a therapeutic vulnerability to ROS-inducing drugs. These data uncover an oncogene vulnerability to ferroptosis caused by increased iron accumulation and subsequent reliance on the system Xc-/GSH pathway.

Keywords

MYCN-amplified neuroblastoma; ferroptosis; glutathione; auranofin; iron accumulation

Introduction

While evasion of apoptosis has been recognized as a hallmark of cancer for fifty years, the involvement of other recognized modes of programmed cell death remains understudied. Ferroptosis is a cell death program identified by Stockwell and colleagues in 2012 (1) that is characterized by accumulation of iron (Fe)-dependent reactive oxygen species (ROS) causing lipid peroxidation related cell death. Morphologically, it is defined by smaller mitochondria, increased density of the mitochondrial membrane, vanishing of the mitochondrial cristae, rupture of the outer mitochondrial membrane and cellular disintegration (2). This form of cell death appears particularly relevant to cancer cells as iron accumulation allows for high activity of iron- and heme-containing enzymes that play roles in diverse processes from cell cycle progression to cellular metabolism (3). For instance, DNA polymerases require iron (4), as do enzymes involved in mitochondrial respiration and the citric acid cycle (5), and ribonucleotide reductase (6). Indeed, oncogenes like *HIF1A* can increase iron metabolism (3). Increased iron metabolism, however, is a double-edged sword as it is a major ROS producer through the Fenton reaction, the donation of an electron from ferrous iron to hydrogen peroxide to produce hydroxyl radicals (OH-) (7). Hydroxyl radicals are counteracted by glutathione peroxidase 4 (GPX4), a powerful cellular ROS scavenger that utilizes glutathione (GSH) to directly prevent lipid peroxidation – the oxidative degradation of lipids. Lipid peroxidation results in ferroptotic cell death (8), and therefore GPX4 is the central preventive molecule of this process (9,10).

While RAS was originally connected to the activity of the ferroptosis inducer erastin (11), interactions of oncogenes with the ferroptotic pathway have not been well-characterized. High-risk neuroblastoma (NB) accounts for upwards of 15% of all pediatric cancer related deaths, despite comprehensive therapy. Among high-risk cases are about ¼

with amplification of the oncogenic *MYCN*. *MYCN* encodes an E-BOX–binding, basic-helix-leucine zipper (bHLH-LZ) transcription factor (12). Despite its undeniable role in neuroblastomagenesis, MYCN remains undruggable. Here in, we uncover a druggable target in *MYCN*-amplified NB. We find MYCN drives a transcriptional rewiring of the iron import receptor and system Xc-, creating a marked reliance on the GSH pathway. We find that *MYCN*-amplified NBs are exquisitely sensitive to targeting this pathway either chemically or genetically and that this pathway is activated by MYCN at least in part to detoxify ROS from excess iron transport. As such, we find repurposing FDA-approved RA drug auranofin and the RA and ulcerative colitis drug SAS are effective against *MYCN*-amplified NB, via targeting antioxidant activity.

Materials and Methods

Cell lines

The cell lines RPE.1, IMR5, SIMA, SMS-SAN, LAN5, NB12, SK-N-BE(2), SK-N-SH, SK-N-DZ, SK-N-AS, and KELLY were from the Molecular Center Therapeutics Laboratory at Massachusetts General Hospital, which performs routine testing of cell lines by single-nucleotide polymorphism and short tandem repeat analysis. The SK-N-FI cell line was provided by the Children's Hospital of Pennsylvania (Y. Mossé). COG-N-415, COG-N-496, CHLA20, and CHLA172 were kindly provided by the Children's Oncology Group (COG) Cell Culture and Xenograft Repository (C. Pat Reynolds and the Texas Tech Health Sciences Center), powered by Alex's Lemonade Stand Foundation. The SK-N-BE(2), SK-N-AS, SK-N-SH, IMR5, SK-N-DZ and SK-N-FI cell lines were cultured in DMEM/F12 (50:50) supplemented with 10% FBS, 1 μg/mL penicillin and streptomycin. The RPE.1, SIMA, KELLY, NB12, LAN5, and SMS-SAN cell lines were cultured in RPMI 1640 supplemented with 10% FBS, 1 μg/mL penicillin and streptomycin. The CHLA20 and CHLA172 cell lines were cultured in DMEM supplemented with 20% FBS, 1× insulin-transferrin-selenium (ITS) (41400045; Thermo Fisher Scientific), 1 μg/mL penicillin and streptomycin. The COG-N-415 and COG-N-496 cell lines were cultured in Iscove's modified Dulbecco's medium supplemented with 20% FBS, 1× ITS, 1 μg/mL penicillin and streptomycin. Cell lines were used for less than 40 passages but were not independently authenticated. They were regularly screened for Mycoplasma using a MycoAlert Mycoplasma Detection Kit (LT07–318; Lonza).

Xenograft Studies

NOD CRISPR Prkdc Il2r Gamma (NCG) male mice were injected with ~5×10^6 IMR5 or SK-N-SH cells per 200 μL of 1:1 (cells: Matrigel (354248; Corning)). Cells were injected on both flanks of the mice and monitored for tumor growth. When tumors reached an average size of 150–200 mm^3, the tumor-bearing mice were randomized (IMR5: no treatment = 4 tumors, auranofin = 6 tumors, sulfasalazine = 3 tumors; SK-N-SH: no treatment = 4 tumors, auranofin = 4 tumors). The tumors were measured every other day by electronic caliper, in two dimensions (length and width), and with the formula $v = l \times (w)2\ (\pi/6)$, where v is the tumor volume, l is the length, and w is the width (the smaller of the two measurements). Mice were treated with auranofin (10 mg/kg/qd/i.p.) (20 μl; DMSO) 6 days/week (Monday to Saturday) or sulfasalazine (250 mg/kg/qd/i.p.) (100 μl; PBS) 6 days/week (Monday to

Saturday) for 13 days (IMR5) or 10 days (SK-N-SH) total. Mice bearing IMR5 or SK-N-SH cell xenografts were euthanized after the 13th and 10th day of the treatment respectively, because some of the tumors of the "control" (no treatment) or auranofin cohort reached or exceeded the size of 1,000 mm^3. All mouse experiments were approved and performed in accordance with the Institutional Animal Care and Use Committee at VCU.

Patient-derived xenograft (PDX) models

The COG-N-561, COG-N-452, COG-N-415 and COG-N-496 PDX models were kindly provided by the Children's Oncology Group (COG) Cell Culture and Xenograft Repository (C. Pat Reynolds and the Texas Tech Health Sciences Center), powered by Alex's Lemonade Stand Foundation, and were injected into NOD CRISPR Prkdc Il2r Gamma (NCG) male mice at 2×10^6 cells per flank on both flanks of the mouse using a 1:1 ratio of cells/Matrigel. Mice were randomized when tumors reached an average size of 150–250 mm^3, (COG-N-561: no treatment = 6 tumors, auranofin = 6 tumors; COG-N-452: no treatment = 6 tumors, auranofin = 4 tumors; COG-N-415: no treatment = 7 tumors, sulfasalazine = 7 tumors, COG-N-496: no treatment = 6 tumors, auranofin = 3 tumors). Mice were treated with auranofin (10 mg/kg/qd/i.p.) (20 μl; DMSO) 6 days/week (Monday to Saturday) for 30 days (COG-N-561) for 16 days (COG-N-452), for 24 days (COG-N-415) or for 11 days (COG-N-496). Mice bearing COG-N-452 as well as COG-N-496 tumors were euthanized after the 16th and 11th day of the treatment respectively, because some of the tumors of the "control" (no treatment) cohort reached (COG-N-452 model) or exceeded (COG-N-496 model) the size of 1,000 mm^3. All animal experiments were approved by the Virginia Commonwealth University (VCU) Institutional Animal Care and Use Committee.

Results

Neuroblastomas are sensitive to genetic and chemical GPX4 inhibition

The phospholipid hydroperoxidase glutathione peroxidase 4 (GPX4) serves as the primary protection of cells from ferroptotic cell death and lipid peroxidation (13), and its genetic inhibition results in ferroptosis (13–15). GPX4 depletion/ferroptosis induction has recently been reported to be a vulnerability of cells that undergo EMT (8,15). Our investigations began when upon examining the Broad Institute depository of three genome-wide siRNA screens (Depmap) covering over 700 hundred cancer cell lines, we noted the highest toxicity observed following GPX4 knockdown was in NB (Fig. 1A and Sup. Fig. 1A); interestingly, most of the NB cell lines had amplification of *MYCN* (Sup. Fig. 1B).

To corroborate these data chemically and to begin to assess a possible role of MYCN in sensitivity, we analyzed within the Depmap consortium, screening data with the GPX4 chemical inhibitor, ML210 (9). Here, we found *MYCN*-amplified NB cells were hypersensitive to pharmaceutical GPX4 inhibition (Fig. 1B), consistent with the genetics data. These data evidenced a sensitivity of *MYCN*-amplified NB to GPX4 inhibition.

Neuroblastomas are vulnerable to disruption of system Xc- receptor/glutathione pathway

Upstream of GPX4 is the antioxidant glutathione (GSH), which enables GPX4 by donating an electron. In turn, GSH synthesis is controlled primarily by the system

Xc- receptor pathway. As *MYCN*-amplified NB were highly represented among the neuroblastoma cancer cell lines in the GPX4 siRNA assay, we hypothesized that MYCN may create a particular vulnerability along the system Xc- pathway/GSH axis. To do so, we interrogated a panel of *MYCN*-amplified NB cell lines and *MYCN*-wild type NB cell lines with buthionine-(S,R)-sulfoximine (BSO), a potent inhibitor of the rate-limiting GSH synthesizing enzyme, gamma-glutamylcysteine synthetase (GGS) (13,16,17). Of significance, we found enhanced sensitivity to BSO in the *MYCN*-amplified NB cell line panel versus the wild-type panel (Fig. 1C). To directly assess whether MYCN sensitizes NB cells to BSO, we expressed exogenous MYCN in *MYCN*-wildtype CHLA20 and SK-N-SH NB cells. The presence of MYCN conferred synthetic lethality to BSO (Fig. 1D). We next knocked down MYCN with siRNA in two *MYCN*-amplified NB cell lines, IMR5 and SK-N-BE(2). In both cases, we found a marked reduction in sensitivity to BSO when MYCN was reduced (Fig. 1E and Sup. Fig. 1C). Consistent with on-target activity, BSO depleted GSH (Fig. 1F), induced ROS (Fig. 1G), and was protected by co-treatment with the antioxidant N-acetyl-L-cysteine (NAC) in *MYCN*-amplified NB cell lines (Fig. 1H and Sup. Fig. 1D). Moreover, BSO-mediated toxicity was protected by the ferroptosis and lipid peroxidation inhibitor a-tocopherol in *MYCN*-amplified NB cell lines (Fig. 1I and Sup. Fig. 1E), demonstrating on-target activity of ferroptotic cell death by BSO. These data indicated a vulnerability to GSH inhibition by MYCN in NB, resulting in ferroptosis.

MYCN upregulates system Xc- in neuroblastoma

The import of cystine serves as the limiting step to synthesize GSH (cystine is reduced to cysteine in the cell) (18). Our data above demonstrate MYCN confers sensitivity to GSH targeting in NB. Based on these data, we hypothesized there is a likeliness that there is a significant influx of cystine that creates high activity of the GSH catabolic pathway. We looked at the two genes that encode the subunits of the system Xc- antiporter, as expression of the receptor is the key hub for controlling cystine import and subsequent activity of this pathway (2). Indeed, we found both genes encoding the heterodimeric system Xc- (*SLC7A11* and *SLC3A2*) were markedly increased in *MYCN*-amplified NB tumors versus *MYCN*-wild-type NB tumors (19) (Fig. 2A). As an oncogenic transcriptional factor, *MYCN* drives expression of target genes that participate in establishing and maintaining a cancerous phenotype. We reasoned due to the increase in expression of the system Xc- receptor subunits, that MYCN may directly bind to and promote transcription of the system Xc- receptor. For this, we parsed data from a study utilizing an elegant system of a *MYCN*-wild-type cell line (SHEP21) (20). This system includes the SHEP21 parental cells, a MYCN negative cell line, and the SHEP21N cells, modified to express exogenous MYCN, and which expression is lost with the addition of doxycycline (20). Indeed, there was marked direct binding of MYCN to *SLC3A2* at canonical E-boxes in the *SLC3A2* promoter in both systems (Fig. 2B), indicating direct transcriptional upregulation by MYCN. Binding of MYCN to the promoter of *SLC7A11* was also present, although not as pronounced (Sup. Fig. 2A). Consistent with the upregulation of the system Xc- receptor in *MYCN*-amplified NB tumors and a direct upregulation of *SLC3A2* by MYCN, exogenous MYCN expression in MYCN wild-type NB cells and the RPE.1 neural crest cell line led to increased protein levels of both SLC7A11 and SLC3A2 (Fig. 2C, *left*). Conversely, silencing *MYCN* in the *MYCN*-amplified KELLY and SK-ND-Z cells results in a significant loss of SLC7A11

and SLC3A2 (Fig. 2C, *right*). While cystine uptake is rate-limiting to GSH synthesis (21), when intracellular cysteine is abundant, the glutamate-cysteine ligase, made up of the GCL catalytic subunit, GCLC, and a modifier subunit, becomes the rate-limiting step towards the biosynthesis of GSH (22). Again, consistent with increased flux through this pathway, we found *MYCN*-amplified NB tumors had higher levels of GCLC compared to wild-type tumors (19,23) (Sup. Fig. 2B) which coincided with increased binding of MYCN to the *GCLC* promoter (20) (Sup. Fig. 2C). Exogenous expression of MYCN was sufficient to increase GCLC expression, while knockdown of endogenous MYCN in the *MYCN*-amplified NB cell lines was sufficient to reduce GCLC (Sup. Fig. 2D).

Increased flux through the system Xc- pathway and increased GCLC suggested MYCN also increased GSH levels. Therefore, in our MYCN syngeneic models, we determined whether there was enhanced GSH production. Indeed, we found GSH levels were higher in the syngeneic models expressing exogenous MYCN and lower in the si *MYCN*-treated models, when compared to their respected controls (Fig. 2C–2E and Sup. Fig. 2D). Altogether, these data demonstrate MYCN orchestrates increased system Xc- expression and subsequent flux through the system Xc-/GSH pathway.

Reducing cystine is toxic in the presence of amplified *MYCN* in NB

We next sought to determine whether this translated to enhanced sensitivity of targeting the system Xc- directly. To do so, we first limited available cystine for the cells in culture, and measured viability in the syngeneic models. As demonstrated in Fig. 2F, cystine deprivation was substantially more toxic to NB cells in the presence of MYCN. Consistent with an enhanced reliance on this pathway for survival, genetic inhibition of *SLC3A2* and *SLC7A11* was sufficient to induce toxicity in *MYCN*-amplified NB lines (Sup Fig. 2E). To assay whether these data together would translate to a pharmaceutical vulnerability, we treated our panel of *MYCN*-amplified and *MYCN*-wild type cells with sulfasalazine (SAS), a system Xc- receptor inhibitor (24). Similar to the results from BSO (Fig. 1C), we found *MYCN*-amplified NB were considerably more sensitive than the *MYCN*-wild-type NB cell lines following therapy with SAS (Fig. 3A), and SAS potently inhibited GSH levels in the *MYCN*-amplified NB cells (Fig. 3B). Consistent with SAS depletion of GSH resulting in ferroptotic cell death, treatment with the ferroptosis inhibitors ferrostatin-1 or liproxstatin-1 resulted in mitigated toxicity (Fig. 3C). Consistent with the notion MYCN was driving sensitivity, we found enhanced sensitivity in the syngeneic models when MYCN was present (Fig. 3D), whereas silencing of MYCN resulted in profound resistance (Fig. 3E and Sup. Fig. 2D); again, ferrostatin-1 prevented SAS toxicity in the si Control-treated *MYCN*-amplified NB cells (Sup. Fig. 2F, 2G and 2H). As SAS is FDA-approved, we evaluated its efficacy *in vivo*. SAS (250 mg/kg, q.d.) was sufficient to block tumor growth in two *MYCN*-amplified NB models (Fig. 3F). In tumor tissue, SAS induced TfR1, as well as malondialdehyde (MDA) (Fig. 3G and Sup. Fig. 3A), a combination of antibodies that are specific ferroptosis markers *in vivo* (25). Additionally, no significant alterations were observed in the expression of SLC3A2 and SLC7A11 (Sup. Fig. 3B). Altogether, MYCN increases system Xc- expression and pathway activation, resulting in a hypersensitivity of *MYCN*-amplified NB to system Xc- receptor targeting.

Iron accumulation is increased in *MYCN*-amplified NB

These data indicated a new therapeutic vulnerability in *MYCN*-amplified NB. We sought to understand the basis for enhanced system Xc- pathway activation and toxicity from genetic or pharmaceutical targeting in *MYCN*-amplified NB. Increased expression of system Xc- suggests a particularly large need for *MYCN*-amplified NB to detoxify ROS. Iron is a major contributor to increased cancer proliferation and survival (26), however, it is also detrimental to the cell as it is a major ROS producer through the Fenton reaction, the donation of an electron from ferrous iron to hydrogen peroxide to produce hydroxyl radicals (OH-). Indeed iron-induced ROS at lipids causes ferroptotic cell death (1).

As sensitivity to GPX4 inhibition is linked to ferroptosis (1,15), this further suggested to us the possibility of aberrant iron accumulation in *MYCN*-amplified NB to drive its proliferative program. To begin to test whether *MYCN* increased iron metabolism in NB, we assessed the reliance of MYCN overexpressing cells on iron accumulation. Indeed, while the *MYCN* wild-type cells showed only modest sensitivity (~25%) to the higher concentrations of the iron scavenger deferoxamine (DFO) used in the dose-response assay, the presence of exogenous *MYCN* conferred susceptibility (Fig. 4A). Consistent with this, the *MYCN*-amplified NB cell lines were more sensitive than the *MYCN*-wild-type NB cell lines (Fig. 4B). Iron is controlled at the receptor level: transferrin is the receptor responsible for iron import, and ferroportin is responsible for iron export (3). We first evaluated the expression of the transferrin receptor (encoded by the *TFRC* gene). In fact, *TFRC* levels were increased in NB tumors with *MYCN* amplification (27) (Fig. 4C). Similar to MYCN binding directly to system Xc- receptors to upregulate its expression, we found, in the SHEP21 system, that MYCN directly binds to E-box sites in the promoter of *TFRC* (Fig. 4D). Interrogation of the syngeneic pairs RPE.1, CHLA20 and CHLA172 by western blotting verified the increase of the transferrin receptor in the MYCN overexpressing cells (Fig. 4E). We next tested whether iron levels were higher when MYCN is present. In line with our hypothesis, there was an increased labile Fe (II) pool in the syngeneic RPE.1 and MYCN-wild type NB cells when in the presence of exogenous MYCN, as demonstrated by a Fe (II) selective probe (Fig. 4F). Although *TFRC* was higher, cellular iron levels are also controlled by the iron export receptor, ferroportin. Indeed, we found expression of ferroportin, (encoded by the *SLC40A1* gene), was lower in *MYCN*-amplified NBs across the tumor datasets (Fig. 4G). These data were also corroborated at the protein level in the syngeneic models (Fig. 4E). As DNA methylation plays a large role in expression patters in NB (28), we interrogated the status of ferroportin methylation across 105 NB tumors (28). Interestingly, we discovered the *SLC40A1* gene had increased methylation along the promoter and first exon in the *MYCN* NBs (Sup. Fig. 4), likely contributing to lower expression in *MYCN*-amplified NB. Therefore, both MYCN-directed *TFRC* expression and a decreased level of the *SLC40A1* gene, encoding the ferroportin iron export receptor, contribute to enhanced iron capture in *MYCN*-amplified NB.

MYCN-amplified NB are sensitive to the FDA-approved auranofin

Amplified *MYCN* drives increased iron accumulation through receptor modulation and enhanced sensitivity to cystine deprivation and system Xc- receptor inhibition. As our goal is for clinical translation, while SAS is FDA-approved, we sought to find an additional clinical

drug that could be immediately translated to NB clinical trials. Of note, the antioxidant thioredoxin reductase, is a powerful ROS detoxifier which along with GSH, are responsible for controlling the redox state of the cell.

We reasoned that *MYCN*-amplified NB would also need this pathway to detoxify the ROS from the increased demands from enhanced iron metabolism. We therefore studied auranofin, an FDA-approved drug for rheumatoid arthritis (RA) (29) that is a potent thioredoxin reductase inhibitor and has recently been repurposed in preclinical studies as an anti-cancer agent by increasing ROS (30). Consistent with this hypothesis and known mode of activity as a thioredoxin reductase inhibitor, we found that auranofin had preferentially activity in *MYCN*-amplified NB (Fig. 5A). The sensitivity auranofin conferred to the *MYCN*-amplified NB cell lines was reversed by the addition of the ferroptosis inhibitor, ferrostatin-1 (Fig. 5B), implementing ferroptosis in the toxicity. The role of MYCN was confirmed in the syngeneic models expressing MYCN compared to those expressing GFP (Fig. 5C). When MYCN was knocked down by short hairpin (sh)RNA (Fig. 5D), or siRNA (Sup. Fig. 5A), auranofin sensitivity was mitigated. The cell viability data were further verified by crystal violet assays demonstrating increased sensitivity in the presence of exogenous MYCN (Sup. Fig. 5B) or when MYCN was knocked down by shRNA (Sup. Fig. 5C). Similar to ferrostatin-1, treatment with NAC mitigated auranofin toxicity in the *MYCN*-amplified IMR5 cells (Sup. Fig. 5D, *left*), and did so in a MYCN-dependent manner (Sup. Fig. 5D, *right*).

To further demonstrate auranofin was preferentially active in *MYCN*-amplified NB by interfering with ROS neutralization, we measured both soluble ROS levels and ROS formed in lipids. Consistent with auranofin-mediated inhibition of thioredoxin reductase as central to its activity, ROS levels tracked with the anti-growth effects of auranofin: in the SK-N-DZ cells, ROS levels only substantially increased at 3330nM, where activity was first seen, but in the KELLY and SIMA cells, ROS levels substantially increased in response to much lower doses (330nM), where auranofin was effective (Fig. 5E and Sup. Fig. 5E). The amount of ROS increased by auranofin was higher in the presence of MYCN, and, importantly, the iron scavenger DFO markedly hindered ROS production by auranofin and to a greater degree in the presence of MYCN (Fig. 5F). Furthermore, the intracellular iron levels were sharply increased with auranofin, which is consistent with GSH level increase (Sup Fig. 5F and Sup. Fig. 5G) from a cellular feedback mechanism when thioredoxin activity is inhibited by auranofin (31). In line with these observations, an increase of SLC7A11 was also displayed at 1000nM of auranofin (Sup. Fig. 5H).

To further probe the relationship between auranofin and iron accumulation in *MYCN*-amplified NB, we co-treated the *ex vivo MYCN*-amplified PDX COG-N-496 cells with auranofin and the iron scavenger DFO. Strikingly, DFO blocked auranofin toxicity in a dose-dependent manner, consistent with ROS generation from iron accumulation driving sensitivity to auranofin (Fig. 5G, *left*). We further tested this relationship in the CHLA20 NB cells with GFP and exogenous MYCN expression. Similar to the enhanced sensitivity in the *MYCN*-amplified NB, MYCN was sufficient to induce sensitivity to DFO, and, strikingly, auranofin efficacy was mitigated by DFO and only in the cells expressing MYCN (Fig. 5H). Although MYCN was insufficient to induce sensitivity to DFO in the CHLA172 syngeneic

line, once again, DFO robustly mitigated auranofin sensitivity, and once again, only in the presence of MYCN (Sup. Fig. 5I). These data strongly infer that auranofin is selectively active in *MYCN*-amplified NB only in the presence of increased iron influx, consistent with our hypothesis.

c-MYC high neuroblastoma are vulnerable to system Xc- inhibition and ferroptosis

High c-MYC is a driver of a distinct subset of high-risk NBs (32), and c-MYC and MYCN share, to an extent, an overlapping transcriptome (33). Thus, we hypothesized that c-MYC should also serve as an activator for the GSH antioxidant pathway and cystine import in NBs. Indeed, consistent with an inverse correlation between MYCN and c-MYC in NB (34), we found the highest c-MYC expressing NB lines in our panel were *MYCN*-wild-type (Sup. Fig. 6A), where SLC3A2 levels were also higher than in the NBs without either MYCN amplification or high c-MYC levels (Sup. Fig. 6A). To directly assess whether c-MYC affects the iron pathway and system Xc- receptor/GSH pathway, we exogenously expressed c-MYC in the RPE.1 and the *MYCN*-wt, c-MYC low, CHLA172 cell line, and investigated potential alterations in the expression of SLC3A2, SLC7A11 and transferrin receptor 1. In line with this hypothesis, there was significant upregulation in the presence of c-MYC in both cell lines of these proteins, except for SLC7A11 protein in the CHLA172 cells (Sup. Fig. 6B and Sup. Fig. 6C). Treatment of both syngeneic cell line models with auranofin revealed significant sensitization of c-MYC overexpressing cells (Sup. Fig. 6B and Sup. Fig. 6C), and, consistent with upregulation of all three proteins in the RPE.1 cells, this effect was greater in the RPE.1 cells than the CHLA172 cells (75% more toxicity in the c-MYC-expressing RPE.1 cells compared to the control cells, with 25% more toxicity in the c-MYC expressing CHLA172 cells compared to control cells). These data demonstrate c-MYC has a similar effect as MYCN on regulating iron uptake and system Xc-/GSH pathway activation and rendering c-MYC high NBs sensitive to ferroptosis-inducing drugs like auranofin.

Auranofin has activity in *MYCN*-amplified patient-derived xenograft models

We next tested auranofin *in vivo*, as dosed previously (35), in three *MYCN*-amplified PDXs and the *MYCN*-amplified IMR5 xenograft model. These tumors were grown in NOD CRISPR Prkdc Il2r Gamma (NCG) mice, and upon reaching 150 −250 mm^3, were randomized, followed by treatment with 10 mg/kg/qd i.p. auranofin or with no drug. Auranofin was sufficient to slow or block tumor growth in all three *MYCN*-amplified PDX models, including the *MYCN*-amplified COG-N-561 PDX model, taken from a patient following chemo-relapse (36) (Fig. 6A). Additional experiment testing auranofin in mice bearing SK-N-SH (*MYCN*-wt) tumors demonstrated that these tumors were resistant to auranofin (Fig. 6A, *right*), consistent with the differential sensitivity of *MYCN*-amplified NB tumors to auranofin. Similar to SAS, evaluation of tumor tissues treated with auranofin demonstrated a robust ferroptotic response (Fig. 6B and Sup Fig. 3A, Sup. Fig. 7). These data demonstrate that a well-tolerated FDA-approved drug may be repurposed to induce ferroptosis in *MYCN*-amplified NBs, adding to SAS as tailored therapies for *MYCN*-amplified NB. Our model is depicted in Fig. 6C.

Discussion

Recently, the therapeutic opportunities to kill cancer cells vulnerable to ferroptosis has been highlighted by two published studies (8,15) which indicated cancer cells that underwent epithelial-to-mesenchymal transition (EMT) were dependent on GPX4 and disruption of GPX4 or treatment with ferroptosis inducers were selectively toxic to this subpopulation of cells. As the field of ferroptosis is still in its infant stages, potential opportunities have not yet been significantly explored.

In this study, we demonstrate that: 1) MYCN primes NB cells for sensitivity to ferroptosis induction through increased iron import, 2) an oncogenic transcription factor (i.e. MYCN) directs in concert the expression of several receptors to create both an iron dependency and subsequent vulnerability to system Xc- receptor/GSH targeting, 3) that a subset of oncogene-driven cancer (i.e. NB characterized by amplified *MYCN*) is hypersensitive to system Xc-/GSH disruption, 4) there exists evidence of an opportunity to exploit these findings with two FDA-approved drugs, SAS and auranofin, both of which induce ferroptosis in PDX and xenograft models of *MYCN*-amplified NB, and 5) sensitivity to ferroptosis induction can also be seen in c-MYC high NB cell lines, which makes up an additional subset of high-risk NB (34), and this potentially through an identical mechanism.

MYCN continues to be one of the most important targets in cancer therapeutics but remains difficult to drug directly. As an oncogenic transcription factor with high levels of expression in NB, MYCN binds throughout the genome to confer oncogenesis (33). Our study highlights a new and, from a therapeutic standpoint, important way MYCN does this, through activation of the Iron import and subsequent system Xc-/GSH axis, by increasing the expression of key receptors governing these processes. The system Xc-/GSH axis is a vital mechanism for cells to detoxify ROS from iron metabolism. Indeed, transferrin receptor is a marker for ferroptosis (25), and GPX4 is the primary defense against ferroptosis (10,13).

The enhanced sensitivity to ROS targeting is conceptually consistent with the study from Wang and colleagues (37) demonstrating MYCN drives glutaminolysis and enhances ROS production. Indeed, MYCN drives glutamine catabolism (38). Therefore, enhanced glutaminolysis in *MYCN*-amplified NB likely also contributes to the high need of detoxification from ROS that is present in *MYCN*-amplified NB.

The important role of iron to drive growth and proliferation in cancer has come under increasing interest. The diverse pathways that contain enzymes requiring iron to function including those found in the TCA cycle, helicases in DNA synthesis, and signaling molecules like nitric oxide synthase (3,26). In breast cancer, low levels of ferroportin (which increases intracellular iron levels) correlated with metastatic relapse in breast cancer patients (39). Glioblastoma stem cells require transferrin to survive (40). In ovarian cancer, targeting iron is sufficient to slow the growth of a genetic mouse model of the disease (41).

In the current study we demonstrated *MYCN*-amplified NB have a reliance on system Xc-, presumably to counteract increased ROS from iron metabolism. Indeed, targeting the GSH pathway results in ferroptotic cell death (42). We identified within the Depmap

portal (43) (Broad Institute), that GPX4 knockdown was, across hundreds of cancer cell lines and dozens of subtypes of cancer, most effective in NB, which was attributed to the *MYCN*-amplified subset. Since GSH has a short half-life, the pool of cysteine (produced by the import and subsequent reduction of cystine) is critical for the antioxidant activity of this pathway (18). Indeed, the uptake of cystine is thought to be the rate-limiting step for GSH production in the cell (21), and we found limiting cystine in cell culture medium is particularly toxic in the presence of MYCN in NB. The Xc- antiporter shuttles in cystine and shuttles out glutamate, and in some cells at least, is the only known transporter that can bring cystine into the cell (44). Targeting this pathway, at the receptor level (with SAS) or the level of GSH biosynthesis (with BSO), has proven effective in several cancer models (24). Indeed, in our study, MYCN demonstrated synthetic lethality with both drugs. These data are consistent with a recent finding in TH-MYCN mice (45), an elegant mouse model of *MYCN*-amplified NB (46), demonstrating enhanced GSH biosynthesis in these mice.

We also demonstrated that auranofin, a thioredoxin reductase inhibitor that is approved for RA, was an effective drug against *MYCN*-amplified NB both *in vitro* and in NB PDX models. Thioredoxin reductase is part of the thioredoxin antioxidant system, a key cellular antioxidant system (47) that works in parallel with the glutathione pathway (47). Consistently, auranofin has recently been shown to increase ROS *in vitro* in NB cells (48) and is a *bona fide* ferroptosis inducer (49). Auranofin can radio-sensitize diverse cancer cells through increased ROS, which was negated by treatment with the ROS scavenger NAC (48). In addition, we found by co-targeting SAS directly *in vivo* was sufficient to block the grown of NB tumors. These data provide two FDA-approved drugs that specifically target *MYCN*-amplified NB. In ongoing experiments by our group we will assess the efficacy of co-targeting both the system Xc- receptor directory with SAS and the thioredoxin antioxidant system with auranofin to determine if there is additive or synergistic activity, as may be expected.

Overall, we demonstrate that overexpressed MYCN increases iron influx and system Xc-/GSH pathway activation directly through upregulation of the key receptors governing these pathways. These data provide novel insights into how MYCN alters the transcriptome in NB to confer growth and survival advantages. These changes create a vulnerability to ferroptosis inducers and outlines a new strategy to treat these cancers with repurposed FDA-approved drugs.

Supplementary Material

Refer to Web version on PubMed Central for supplementary material.

Acknowledgements

This work was supported by a National Cancer Institute award (R01CA215610) to A.C.F. and an American Cancer Society Research Scholar Grant (RSG-16-013) to A.C.F. Services and products in support of the research project were generated by the Virginia Commonwealth University Cancer Mouse Models Core Laboratory, supported, in part, with funding to the Massey Cancer Center from NIH-NCI Cancer Center Support Grant P30 CA016059.

References

1. Dixon SJ, Lemberg KM, Lamprecht MR, Skouta R, Zaitsev EM, Gleason CE, et al. Ferroptosis: an iron-dependent form of nonapoptotic cell death. Cell 2012;149:1060–72 [PubMed: 22632970]
2. Seibt TM, Proneth B, Conrad M. Role of GPX4 in ferroptosis and its pharmacological implication. Free Radic Biol Med 2019;133:144–52 [PubMed: 30219704]
3. Torti SV, Torti FM. Iron and cancer: more ore to be mined. Nat Rev Cancer 2013;13:342–55 [PubMed: 23594855]
4. Netz DJ, Stith CM, Stumpfig M, Kopf G, Vogel D, Genau HM, et al. Eukaryotic DNA polymerases require an iron-sulfur cluster for the formation of active complexes. Nat Chem Biol 2011;8:125–32 [PubMed: 22119860]
5. Oexle H, Gnaiger E, Weiss G. Iron-dependent changes in cellular energy metabolism: influence on citric acid cycle and oxidative phosphorylation. Biochim Biophys Acta 1999;1413:99–107 [PubMed: 10556622]
6. Thelander L, Graslund A, Thelander M. Continual presence of oxygen and iron required for mammalian ribonucleotide reduction: possible regulation mechanism. Biochem Biophys Res Commun 1983;110:859–65 [PubMed: 6340669]
7. Kajarabille N, Latunde-Dada GO. Programmed Cell-Death by Ferroptosis: Antioxidants as Mitigators. Int J Mol Sci 2019;20
8. Viswanathan VS, Ryan MJ, Dhruv HD, Gill S, Eichhoff OM, Seashore-Ludlow B, et al. Dependency of a therapy-resistant state of cancer cells on a lipid peroxidase pathway. Nature 2017;547:453–7 [PubMed: 28678785]
9. Zou Y, Palte MJ, Deik AA, Li H, Eaton JK, Wang W, et al. A GPX4-dependent cancer cell state underlies the clear-cell morphology and confers sensitivity to ferroptosis. Nature communications 2019;10:1617
10. Forcina GC, Dixon SJ. GPX4 at the Crossroads of Lipid Homeostasis and Ferroptosis. Proteomics 2019;19:e1800311
11. Dolma S, Lessnick SL, Hahn WC, Stockwell BR. Identification of genotype-selective antitumor agents using synthetic lethal chemical screening in engineered human tumor cells. Cancer cell 2003;3:285–96 [PubMed: 12676586]
12. Huang M, Weiss WA. Neuroblastoma and MYCN. Cold Spring Harb Perspect Med 2013;3:a014415
13. Yang WS, SriRamaratnam R, Welsch ME, Shimada K, Skouta R, Viswanathan VS, et al. Regulation of ferroptotic cancer cell death by GPX4. Cell 2014;156:317–31 [PubMed: 24439385]
14. Friedmann Angeli JP, Schneider M, Proneth B, Tyurina YY, Tyurin VA, Hammond VJ, et al. Inactivation of the ferroptosis regulator Gpx4 triggers acute renal failure in mice. Nature cell biology 2014;16:1180–91 [PubMed: 25402683]
15. Hangauer MJ, Viswanathan VS, Ryan MJ, Bole D, Eaton JK, Matov A, et al. Drug-tolerant persister cancer cells are vulnerable to GPX4 inhibition. Nature 2017;551:247–50 [PubMed: 29088702]
16. Cao JY, Dixon SJ. Mechanisms of ferroptosis. Cell Mol Life Sci 2016;73:2195–209 [PubMed: 27048822]
17. Sedlak TW, Paul BD, Parker GM, Hester LD, Snowman AM, Taniguchi Y, et al. The glutathione cycle shapes synaptic glutamate activity. Proc Natl Acad Sci U S A 2019;116:2701–6 [PubMed: 30692251]
18. Lo M, Wang YZ, Gout PW. The x(c)- cystine/glutamate antiporter: a potential target for therapy of cancer and other diseases. J Cell Physiol 2008;215:593–602 [PubMed: 18181196]
19. Kocak H, Ackermann S, Hero B, Kahlert Y, Oberthuer A, Juraeva D, et al. Hox-C9 activates the intrinsic pathway of apoptosis and is associated with spontaneous regression in neuroblastoma. Cell Death Dis 2013;4:e586 [PubMed: 23579273]
20. Zeid R, Lawlor MA, Poon E, Reyes JM, Fulciniti M, Lopez MA, et al. Enhancer invasion shapes MYCN-dependent transcriptional amplification in neuroblastoma. Nature genetics 2018;50:515–23 [PubMed: 29379199]

21. Jefferies H, Coster J, Khalil A, Bot J, McCauley RD, Hall JC. Glutathione. ANZ J Surg 2003;73:517–22 [PubMed: 12864828]
22. Harris IS, Treloar AE, Inoue S, Sasaki M, Gorrini C, Lee KC, et al. Glutathione and thioredoxin antioxidant pathways synergize to drive cancer initiation and progression. Cancer cell 2015;27:211–22 [PubMed: 25620030]
23. Ackermann S, Cartolano M, Hero B, Welte A, Kahlert Y, Roderwieser A, et al. A mechanistic classification of clinical phenotypes in neuroblastoma. Science 2018;362:1165–70 [PubMed: 30523111]
24. Gout PW, Buckley AR, Simms CR, Bruchovsky N. Sulfasalazine, a potent suppressor of lymphoma growth by inhibition of the x(c)- cystine transporter: a new action for an old drug. Leukemia 2001;15:1633–40 [PubMed: 11587223]
25. Feng H, Schorpp K, Jin J, Yozwiak CE, Hoffstrom BG, Decker AM, et al. Transferrin Receptor Is a Specific Ferroptosis Marker. Cell reports 2020;30:3411–23.e7 [PubMed: 32160546]
26. Torti SV, Manz DH, Paul BT, Blanchette-Farra N, Torti FM. Iron and Cancer. Annu Rev Nutr 2018;38:97–125 [PubMed: 30130469]
27. Rajbhandari P, Lopez G, Capdevila C, Salvatori B, Yu J, Rodriguez-Barrueco R, et al. Cross-Cohort Analysis Identifies a TEAD4-MYCN Positive Feedback Loop as the Core Regulatory Element of High-Risk Neuroblastoma. Cancer discovery 2018;8:582–99 [PubMed: 29510988]
28. Henrich KO, Bender S, Saadati M, Dreidax D, Gartlgruber M, Shao C, et al. Integrative Genome-Scale Analysis Identifies Epigenetic Mechanisms of Transcriptional Deregulation in Unfavorable Neuroblastomas. Cancer research 2016;76:5523–37 [PubMed: 27635046]
29. Messori L, Marcon G. Gold complexes in the treatment of rheumatoid arthritis. Met Ions Biol Syst 2004;41:279–304 [PubMed: 15206120]
30. Fidyt K, Pastorczak A, Goral A, Szczygiel K, Fendler W, Muchowicz A, et al. Targeting the thioredoxin system as a novel strategy against B-cell acute lymphoblastic leukemia. Mol Oncol 2019;13:1180–95 [PubMed: 30861284]
31. Yan X, Zhang X, Wang L, Zhang R, Pu X, Wu S, et al. Inhibition of Thioredoxin/Thioredoxin Reductase Induces Synthetic Lethality in Lung Cancers with Compromised Glutathione Homeostasis. Cancer Res 2019;79:125–32 [PubMed: 30401714]
32. Rosswog C, Schmidt R, Oberthuer A, Juraeva D, Brors B, Engesser A, et al. Molecular Classification Substitutes for the Prognostic Variables Stage, Age, and MYCN Status in Neuroblastoma Risk Assessment. Neoplasia 2017;19:982–90 [PubMed: 29091799]
33. Westermann F, Muth D, Benner A, Bauer T, Henrich KO, Oberthuer A, et al. Distinct transcriptional MYCN/c-MYC activities are associated with spontaneous regression or malignant progression in neuroblastomas. Genome Biol 2008;9:R150 [PubMed: 18851746]
34. Zimmerman MW, Liu Y, He S, Durbin AD, Abraham BJ, Easton J, et al. MYC Drives a Subset of High-Risk Pediatric Neuroblastomas and Is Activated through Mechanisms Including Enhancer Hijacking and Focal Enhancer Amplification. Cancer discovery 2018;8:320–35 [PubMed: 29284669]
35. Mirabelli CK, Johnson RK, Sung CM, Faucette L, Muirhead K, Crooke ST. Evaluation of the in vivo antitumor activity and in vitro cytotoxic properties of auranofin, a coordinated gold compound, in murine tumor models. Cancer research 1985;45:32–9 [PubMed: 3917372]
36. Lochmann TL, Powell KM, Ham J, Floros KV, Heisey DAR, Kurupi RIJ, et al. Targeted inhibition of histone H3K27 demethylation is effective in high-risk neuroblastoma. Sci Transl Med 2018;10
37. Wang T, Liu L, Chen X, Shen Y, Lian G, Shah N, et al. MYCN drives glutaminolysis in neuroblastoma and confers sensitivity to an ROS augmenting agent. Cell Death Dis 2018;9:220 [PubMed: 29445162]
38. Qing G, Li B, Vu A, Skuli N, Walton ZE, Liu X, et al. ATF4 regulates MYC-mediated neuroblastoma cell death upon glutamine deprivation. Cancer cell 2012;22:631–44 [PubMed: 23153536]
39. Pinnix ZK, Miller LD, Wang W, D'Agostino R, Jr., Kute T, Willingham MC, et al. Ferroportin and iron regulation in breast cancer progression and prognosis. Sci Transl Med 2010;2:43ra56

40. Schonberg DL, Miller TE, Wu Q, Flavahan WA, Das NK, Hale JS, et al. Preferential Iron Trafficking Characterizes Glioblastoma Stem-like Cells. Cancer cell 2015;28:441–55 [PubMed: 26461092]
41. Basuli D, Tesfay L, Deng Z, Paul B, Yamamoto Y, Ning G, et al. Iron addiction: a novel therapeutic target in ovarian cancer. Oncogene 2017;36:4089–99 [PubMed: 28319068]
42. Miess H, Dankworth B, Gouw AM, Rosenfeldt M, Schmitz W, Jiang M, et al. The glutathione redox system is essential to prevent ferroptosis caused by impaired lipid metabolism in clear cell renal cell carcinoma. Oncogene 2018;37:5435–50 [PubMed: 29872221]
43. Tsherniak A, Vazquez F, Montgomery PG, Weir BA, Kryukov G, Cowley GS, et al. Defining a Cancer Dependency Map. Cell 2017;170:564–76 e16 [PubMed: 28753430]
44. Chung WJ, Lyons SA, Nelson GM, Hamza H, Gladson CL, Gillespie GY, et al. Inhibition of cystine uptake disrupts the growth of primary brain tumors. J Neurosci 2005;25:7101–10 [PubMed: 16079392]
45. Carter DR, Sutton SK, Pajic M, Murray J, Sekyere EO, Fletcher J, et al. Glutathione biosynthesis is upregulated at the initiation of MYCN-driven neuroblastoma tumorigenesis. Mol Oncol 2016;10:866–78 [PubMed: 26996379]
46. Hansford LM, Thomas WD, Keating JM, Burkhart CA, Peaston AE, Norris MD, et al. Mechanisms of embryonal tumor initiation: distinct roles for MycN expression and MYCN amplification. Proc Natl Acad Sci U S A 2004;101:12664–9 [PubMed: 15314226]
47. Lu J, Holmgren A. The thioredoxin antioxidant system. Free Radic Biol Med 2014;66:75–87 [PubMed: 23899494]
48. Krabbendam IE, Honrath B, Bothof L, Silva-Pavez E, Huerta H, Penaranda Fajardo NM, et al. SK channel activation potentiates auranofin-induced cell death in glio- and neuroblastoma cells. Biochem Pharmacol 2020;171:113714
49. Yang L, Wang H, Yang X, Wu Q, An P, Jin X, et al. Auranofin mitigates systemic iron overload and induces ferroptosis via distinct mechanisms. Signal transduction and targeted therapy 2020;5:138 [PubMed: 32732975]

Statement of significance:

The current study shows how MYCN increases intracellular iron levels and subsequent GSH pathway activity and demonstrates the anti-tumor activity of FDA-approved SAS and auranofin in patient-derived xenograft models of MYCN-amplified neuroblastoma.

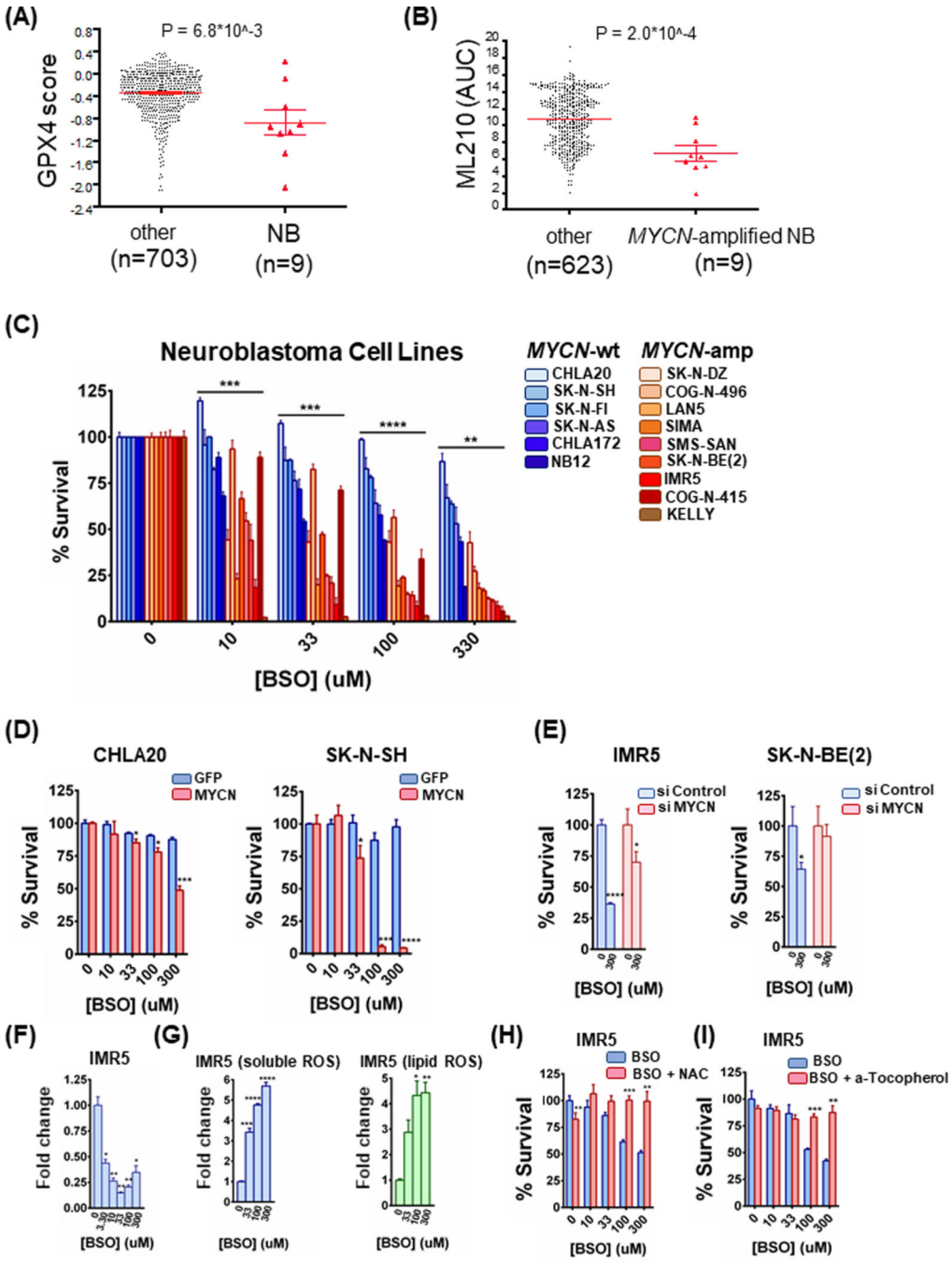

Figure 1. *MYCN*-amplified neuroblastomas (NBs) are hypersensitive to glutathione inhibition.

(**A**) and (**B**) DEPMAP (Broad Institute consortium) analysis of three siRNA screens covering 712 cancer cell lines. Only NBs were uniquely sensitive among all cancer subsets **(A)** and *MYCN*-amplified NB cell lines demonstrated hypersensitivity to the ML210 GPX4 inhibitor (compared to all other cancer cell lines) **(B).** For the dot plots, non-parametric Mann-Whitney test was performed. (**C**) A panel of *MYCN*-amplified and *MYCN*-wild type NB cell lines were treated with increasing concentrations of BSO for 72h and the percentage of viable cells was determined by CellTiter-Glo assay, n=3, error bars indicate +SD. Two-

way Anova test was performed for each concentration separately to determine the effect of the different cell lines as well as the effect of the *MYCN* status for each concentration. p-values were corrected for multiple testing using Bonferroni method. Differences were considered statistically different if $p < 0.05$, * $p < 0.05$, ** $p < 0.01$, *** $p < 0.001$, **** $p < 0.0001$. (**D**) CHLA20 and SK-N-SH control as well as MYCN overexpressing cells were treated with increasing concentrations of BSO for 72h and 48h respectively and cell viability was measured by CellTiter-Glo, $n=3$, error bars indicate +SD. **(E)** IMR5 and SK-N-BE(2) *MYCN*-amplified neuroblastomas were treated with 50 nM scrambled or *MYCN*-targeting siRNA for 24 h. Cells were reseeded and treated the following day with BSO for 48h and cell viability was measured by CellTiter-Glo, $n=3$, error bars indicate +SD. **(F)** Measurement of GSH in IMR5 cells with increasing concentrations of BSO for 72h. Data are means ± SEM with $n=3$ biological replicates. **(G)** IMR5 cells were treated with increasing concentrations of BSO for 48h and stained with CM-H2DCFDA and C-11 BODIPY to mark general and lipid oxidative stress respectively, $n=3$, error bars indicate +SEM. **(H)** IMR5 cells were treated with increasing concentrations of BSO with or without 5 mM N-acetyl-cysteine (NAC) for 48h and cell viability was determined, $n=3$, error bars indicate +SD. **(I)** IMR5 cells were treated with increasing concentrations of BSO alone or in combination with 1 μM a-tocopherol for 48h and cell viability was evaluated, $n=3$, error bars indicate +SD. For figures 1D-1I, Student's *t* test was performed, and p-values were corrected for multiple testing using Bonferroni method. Differences were considered statistically different if $p < 0.05$. For all calculated p-values: * $p < 0.05$, ** $p < 0.01$, *** $p < 0.001$, **** $p < 0.0001$.

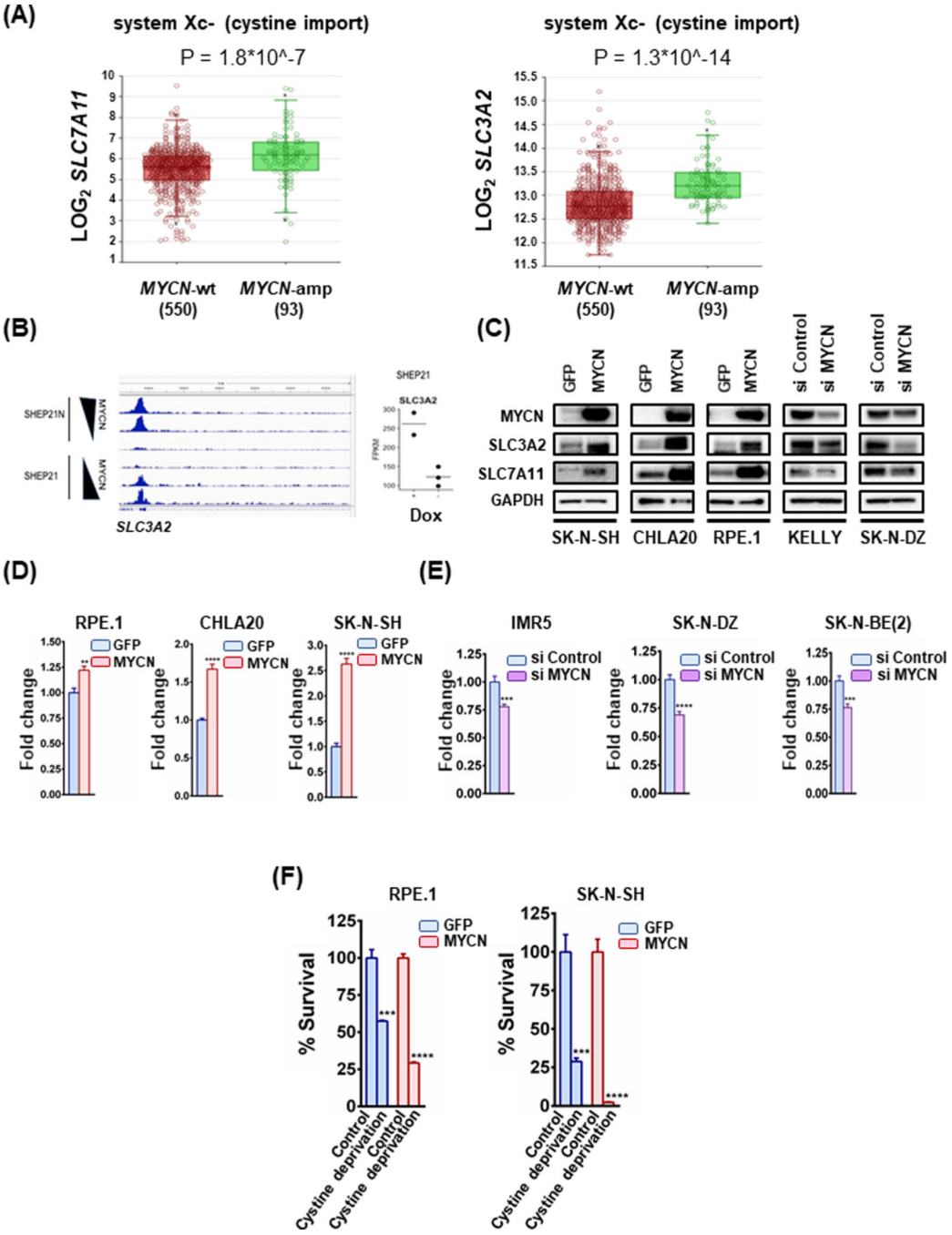

Figure 2. Subunits of the cystine/glutamate antiporter system Xc- are significantly increased in *MYCN*-amplified compared to the *MYCN*-wild type NBs.

(**A**) Box plots from datasets obtained from R2 platform demonstrating differential RNA expression of system Xc- subunits *SLC7A11* and *SLC3A2* in *MYCN*-amplified NB tumors compared to *MYCN*-wt NB tumors. Mann-Whitney test was performed. **(B)** ***on the left*** SHEP21N, a NB cell line engineered to express MYCN in the absence of doxycycline, demonstrates *SLC3A2* promoter binding at an EBOX-positive portion of the promoter, which decreases as MYCN expression does (through the addition of doxycycline). The

SHEP21 cells engineered to express MYCN with the addition of Dox demonstrated a nearly identical peak when MYCN is turned on (Dox is added). **(B)** ***on the right*** Expression data from the SHEP21 cells in MYCN-expression (Dox +) and MYCN-non expression (Dox -) conditions. Each dot represents an independent data point. Statistical analysis was performed using Student's *t* test and p-value was calculated (0.0799), $n=3$. **(C)** Whole cell lysates from *MYCN*-wt NB cell lines expressing either GFP or exogenous MYCN and *MYCN*-amplified NB cells treated with either 50 nM scrambled or 50 nM MYCN-targeting siRNA for 24h were prepared, subjected to western blotting and probed for the indicated proteins. **(D)** Glutathione levels were determined in MYCN overexpressing *MYCN*-wt cell lines along with their GFP overexpressing counterparts. Data are means ± SEM with $n=3$ biological replicates. **(E)** Glutathione levels were detected in *MYCN*-amplified cell lines treated with either 50 nM scrambled or 50 nM MYCN-targeting siRNA. Data are means ± SEM with $n=3$ biological replicates. Lysates from the same cells were used also for Fig. 2C and Sup. Fig. 2D. **(F)** Cystine depletion was carried out in RPE.1 and SK-N-SH syngeneic cell lines for 8 and 24 hours respectively and cell viability was evaluated, $n=3$, error bars indicate +SEM. For figures 2D-2F, Student's *t* test was performed, and p-values were corrected for multiple testing using Bonferroni method. Differences were considered statistically different if $p < 0.05$. For all calculated p-values: * $p < 0.05$, ** $p < 0.01$, *** $p < 0.001$, **** $p < 0.0001$.

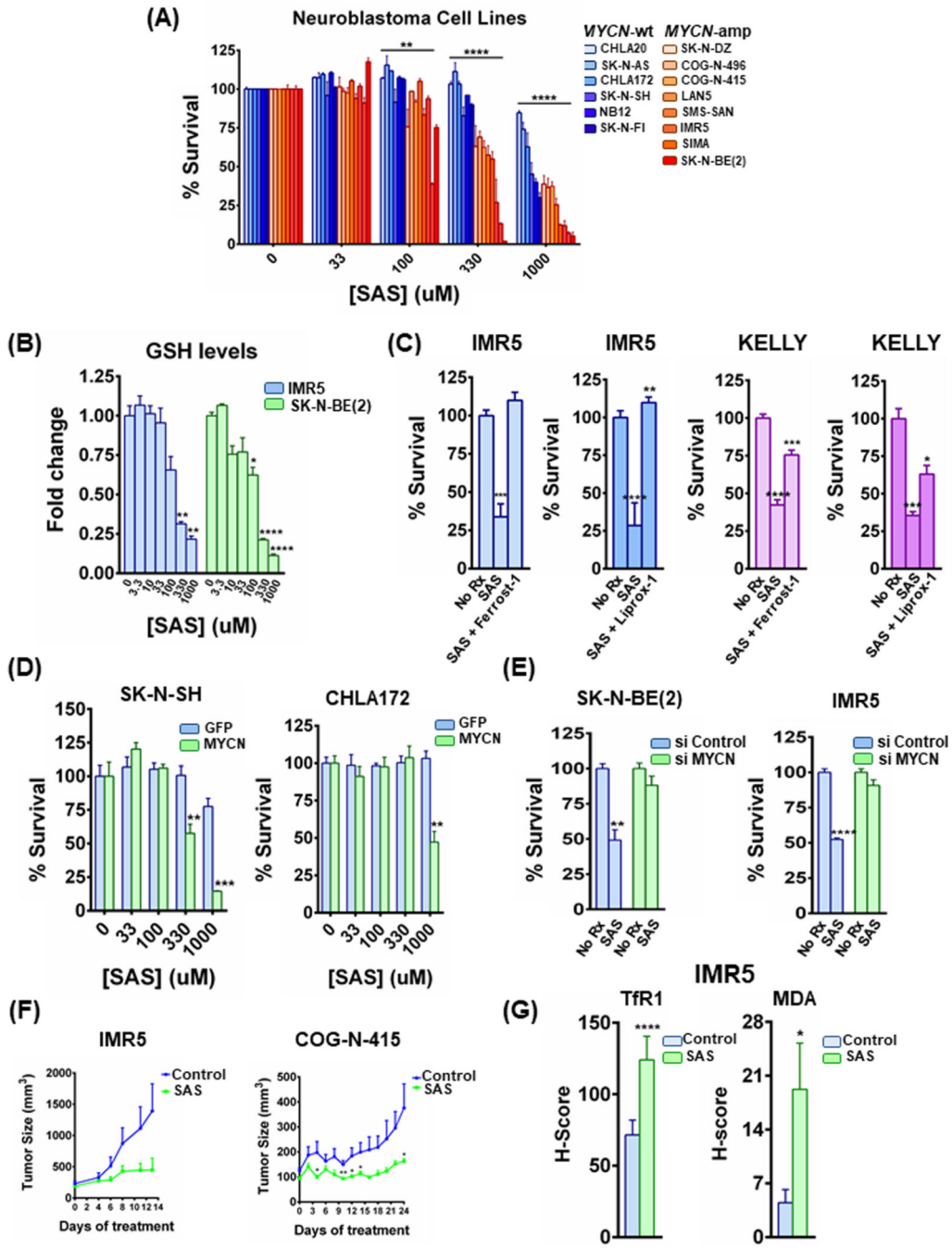

Figure 3. The system xc- inhibitor sulfasalazine induces ferroptosis specifically in *MYCN*-amplified neuroblastoma cells *in vitro* and promotes tumor responses *in vivo*.

(A) *MYCN*-amplified and *MYCN*-wild type cell lines, were treated with increasing concentrations of sulfasalazine (SAS) for 72h and cell viability was detected by CellTiter-Glo, n=3, error bars indicate +SD. Two-way Anova test was performed for each concentration separately to determine the effect of the different cell lines as well as the effect of the *MYCN* status for each concentration. p-values were corrected for multiple testing using Bonferroni method. Differences were considered statistically different if p <

0.05, * p < 0.05, ** p < 0.01, *** p < 0.001, **** p < 0.0001. **(B)** IMR5 and SK-N-BE(2) *MYCN*-amplified cells were treated with increasing concentrations of SAS for 48h and GSH levels were measured by GSH-Glo assay kit from Promega. Data are means ± SEM with n=3 biological replicates. **(C)** KELLY and IMR5 *MYCN*-amplified NB cells were treated with 1mM of SAS or 1mM of SAS together with 10μM of ferrostatin-1 and 10 μM of liproxstatin-1 for 24h (KELLY) and 48h (IMR5) and cell viability was detected, n=3, error bars indicate +SD. **(D)** Syngeneic SK-N-SH and CHLA172 cells were treated with increasing concentrations of sulfasalazine (SAS) for 48h and cell viability was measured by CellTiter-Glo assay, n=3, error bars indicate +SD. **(E)** *MYCN*-amplified cell lines treated with 1 mM of SAS for 48h after being transfected with siRNA against *MYCN* or non-targeting siRNA. Cell viability was assessed as before, n=3 biological replicates, error bars indicate +SD. Lysates from the same cells were used also for Sup. Fig. 2D. **(F)** *MYCN*-amplified NB cell line xenograft (IMR5) as well as PDX model (COG-N-415), were randomized into treatment cohorts as described in the Material and Methods section. Sulfasalazine was administered intraperitoneally, at a dosage of 250 mg/kg, six days a week (Monday-Saturday). Tumor measurements were performed every other day by calipers, and the average tumor volume + SEM for each cohort is displayed. **(G)** The ferroptosis markers transferrin receptor 1 (TfR1) and malondialdehyde (MDA) in control and sulfasalazine treated IMR5 xenografts were detected by immunohistochemistry and their staining was quantified, error bars indicate +SEM. For figures 3B-3G, Student's *t* test was performed, and p-values were corrected for multiple testing using Bonferroni method. Differences were considered statistically different if p < 0.05. For all calculated p-values: * p < 0.05, ** p < 0.01, *** p < 0.001, **** p < 0.0001.

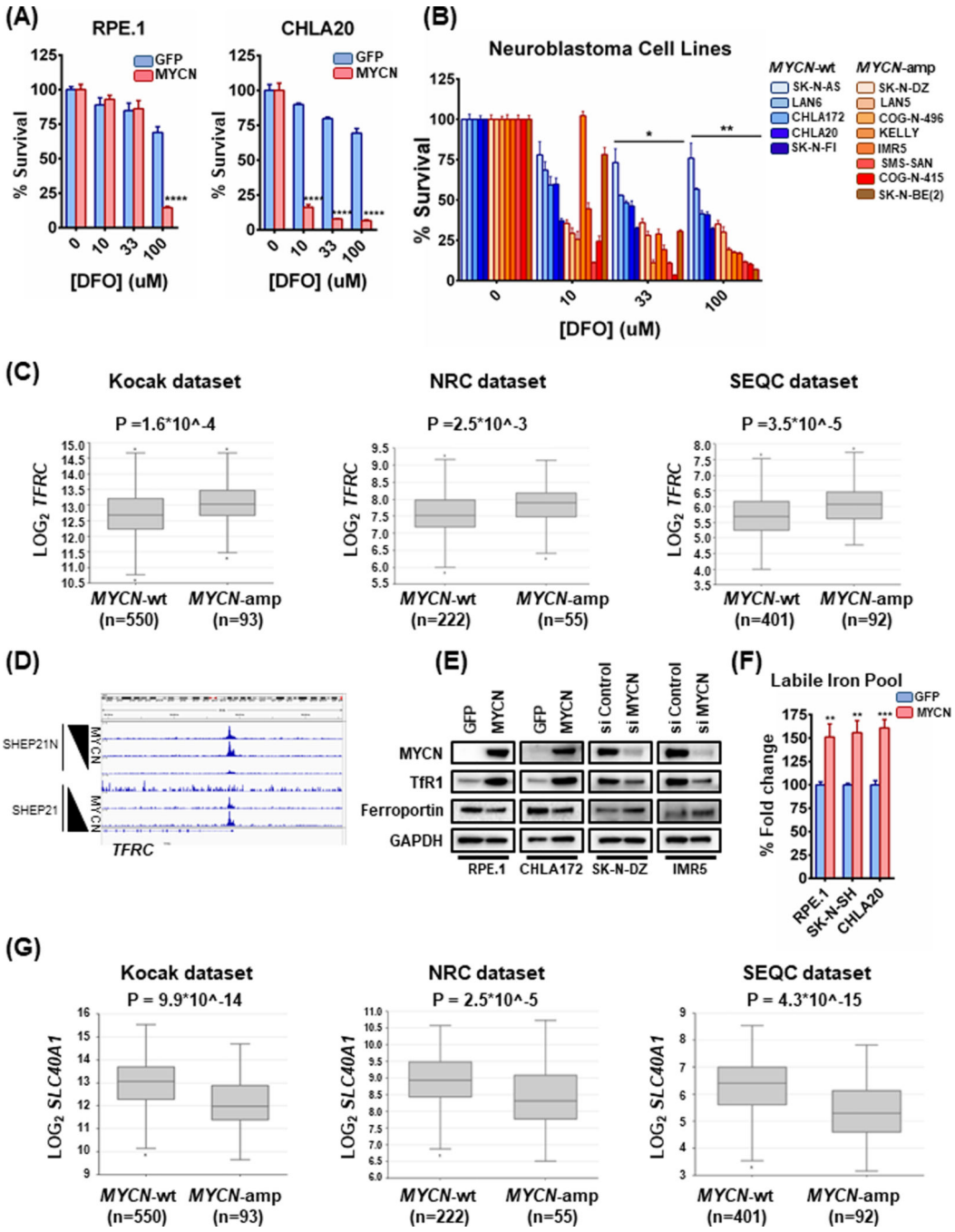

Figure 4. Iron accumulation is increased in *MYCN*-amplified NB.

(A) The CHLA20 and RPE.1 syngeneic pairs were treated with increasing concentrations of deferoxamine (DFO) for 72h and cell viability was assessed by CellTiter-Glo, n=3, error bars indicate +SD. **(B)** Panels of *MYCN*-amplified and *MYCN*-wild type cell lines were treated with increasing concentrations of deferoxamine (DFO) for 72h and cell viability was detected by CellTiter-Glo, n=3, error bars indicate +SD. Two-way Anova test was performed for each concentration separately, to determine the effect of the different cell lines as well as the effect of the *MYCN* status for each concentration. p-values were corrected for

multiple testing using Bonferroni method. Differences were considered statistically different if $p < 0.05$, * $p < 0.05$, ** $p < 0.01$, *** $p < 0.001$, **** $p < 0.0001$. **(C)** Box plots from three distinct NB tumor datasets obtained from R2 platform demonstrating differential *TFRC* mRNA expression levels between *MYCN*-wild type and *MYCN*-amplified NBs. For statistical analysis Mann-Whitney test was performed. **(D)** Same cell line system used in 2B, here used for investigating whether MYCN is binding to the *TFRC* promoter. **(E)** Whole cell lysates from *MYCN*-wt NB cell lines overexpressing exogenous MYCN or GFP or *MYCN*-amplified NB cell lines treated with either 50 nM scrambled or 50 nM MYCN-targeting siRNA for 24h were prepared, subjected to western blotting and probed for the indicated proteins. **(F)** Cellular levels of labile Fe (II) were depicted as percentage change of the average fluorescence intensity between control and MYCN overexpressing syngeneic cell lines using FeRhoNox-1 probe. The values were normalized to the number of live cells measured by CellTiter-Glo, $n=3$, error bars indicate +SEM. **(G)** Box plots demonstrating differential *SLC40A1* mRNA expression levels between *MYCN*-wild type and *MYCN*-amplified NBs across three distinct NB tumor datasets obtained from R2 platform. For statistical analysis Mann-Whitney test was performed. For figures 4A and 4F, Student's *t* test was performed, and p-values were corrected for multiple testing using Bonferroni method. Differences were considered statistically different if $p < 0.05$. For all calculated p-values: * $p < 0.05$, ** $p < 0.01$, *** $p < 0.001$, **** $p < 0.0001$.

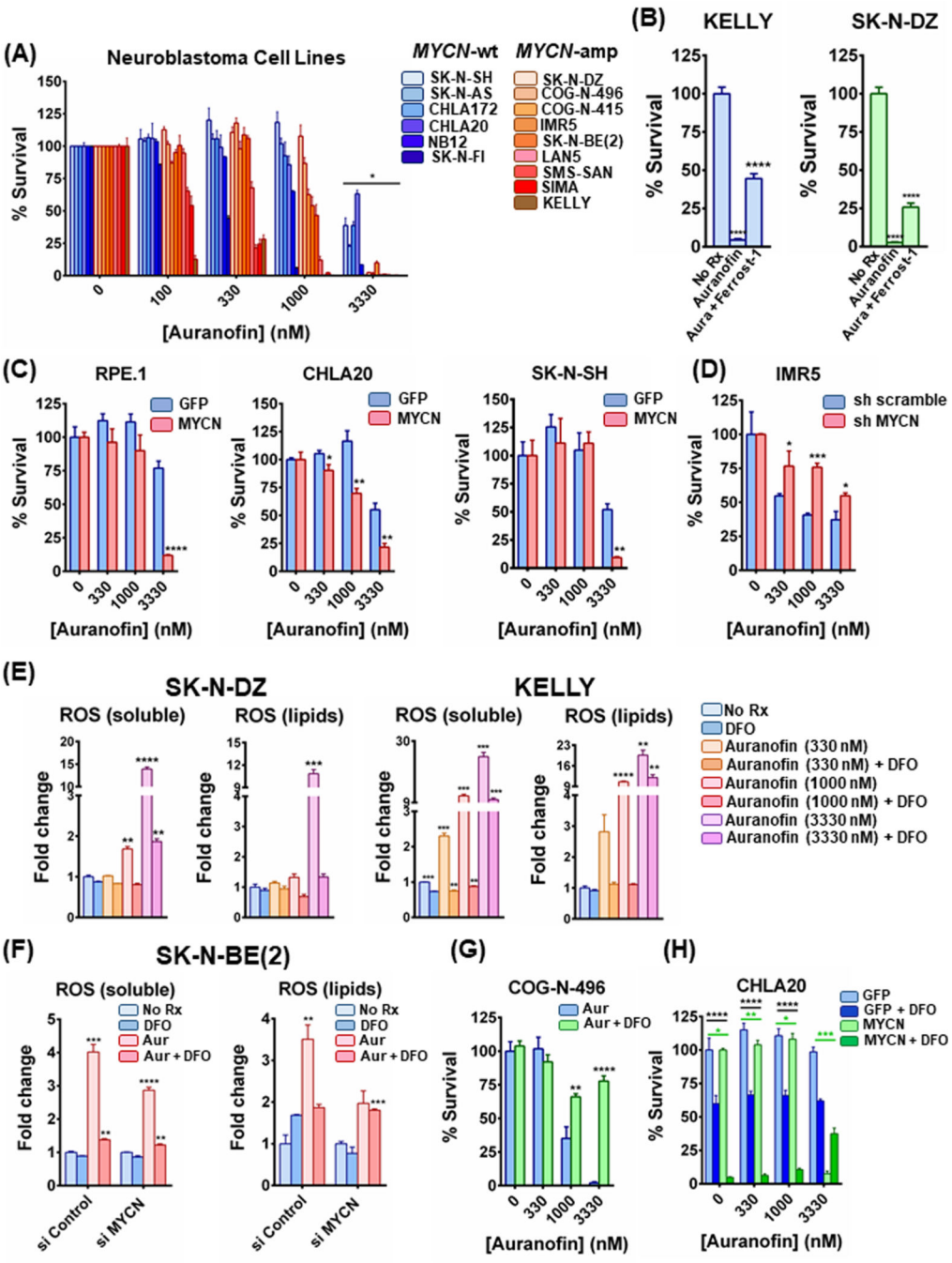

Figure 5. FDA-approved auranofin induces ferroptosis specifically in *MYCN*-amplified NB *in vitro* and promotes tumor responses *in vivo*.

(A) A panel of *MYCN*-amplified and a panel of *MYCN*-wild type NB cell lines were treated with increasing concentrations of auranofin for 72h and the percentage of viable cells was measured by CellTiter-Glo assay, n=3, error bars indicate +SD. Non-parametric Mann-Whitney test was performed for each concentration separately, comparing cell viability values between *MYCN*-wt and *MYCN*-amplified cell lines. Differences were considered statistically different if $p < 0.05$. **(B)** KELLY and SK-N-DZ *MYCN*-amplified NB cells

were treated with 3300 nM of auranofin or 3300 nM of auranofin together with 10μM of ferrostatin-1 overnight and cell viability was detected, n=3, error bars indicate +SD. **(C)** RPE.1, CHLA20 and SK-N-SH syngeneic models expressing MYCN and GFP were treated with increasing concentrations of auranofin for 48h, 72h and 12h respectively and CellTiter-Glo assay was performed, n=3, error bars indicate +SD. **(D)** Additionally, IMR5 cells were transduced with lentiviruses containing plasmids with shRNA sequences targeting *MYCN* or a nontargeting control. Puromycin-resistant cells were pooled after each infection. Both sh *MYCN* and sh *Scramble* cells were also treated with increasing concentrations of auranofin for 12h and cell viability was assessed, n=3, error bars indicate +SD. **(E)** KELLY and SK-N-DZ cells were treated with increasing concentrations of auranofin with or without 100 μM DFO for 5h and stained with CM-H2DCFDA and C-11 BODIPY to mark general and lipid oxidative stress respectively, n=3, error bars indicate +SEM. **(F)** *MYCN*-amplified SK-N-BE(2) cells were treated with 50 nM scrambled or *MYCN*-targeting siRNA for 24 h. Cells were reseeded and treated the following day with 3300 nM auranofin alone or in the presence of 100 μM DFO for 3h and intracellular as well as lipid ROS levels were measured, n=3, error bars indicate +SEM. **(G)** and **(H)** Ex vivo *MYCN*-amplified PDX cells COG-N-496 as well as the syngeneic CHLA20 pair were treated with increasing concentrations of auranofin in combination with 100 μM DFO overnight (COG-N-496) or for 48h (CHLA20 MYCN/GFP) and the percentage of viable cells was detected by CellTiter-Glo, n=3, error bars indicate +SD. For figures 5B-5G, Student's t test was performed, and p-values were corrected for multiple testing using Bonferroni method. For figure 5H, two-way Anova test was performed for each concentration separately; the comparisons between GFP and MYCN are depicted with green color and the comparisons between −/+ DFO with black color. Differences were considered statistically different if $p < 0.05$. For all calculated p-values: * $p < 0.05$, ** $p < 0.01$, *** $p < 0.001$, **** $p < 0.0001$.

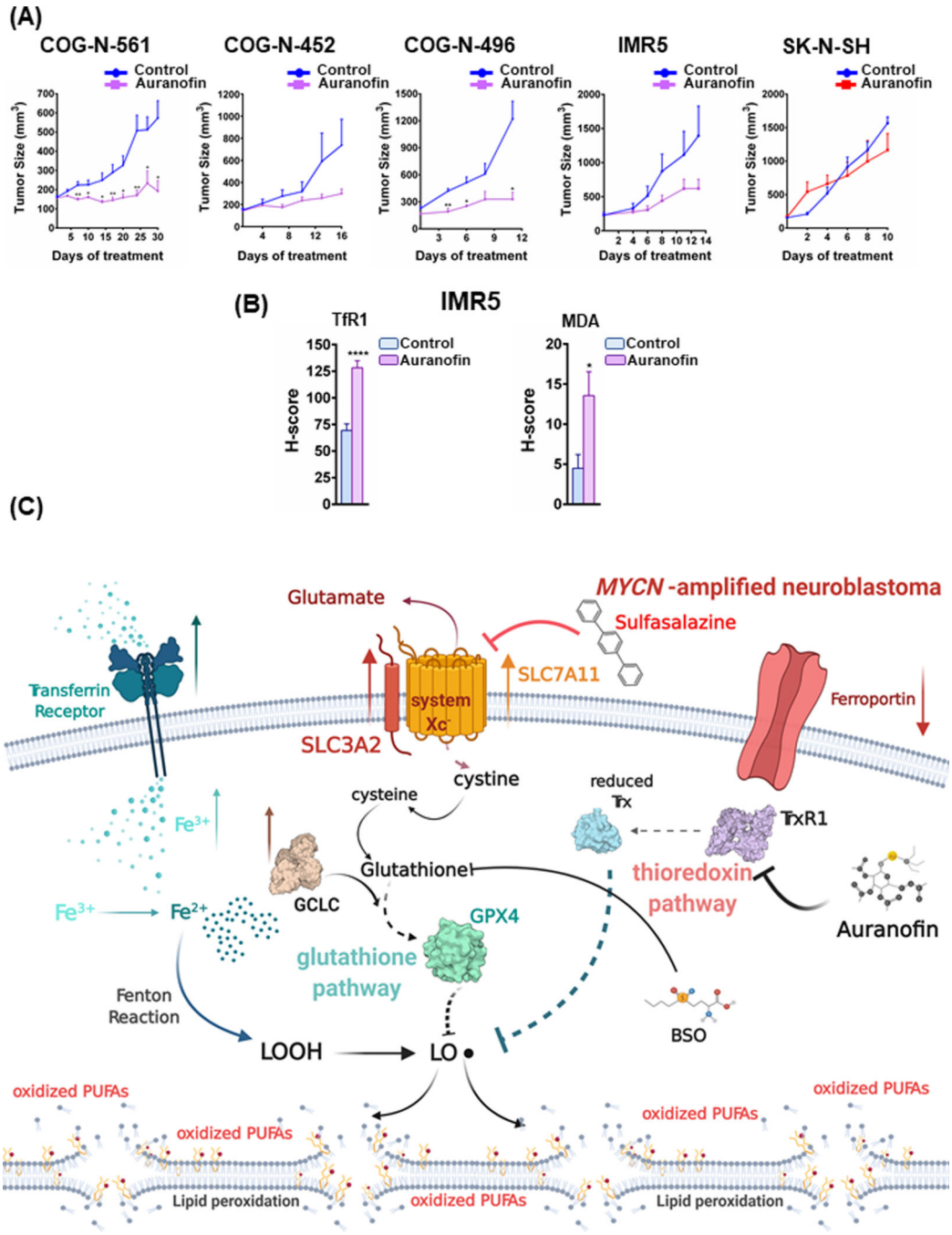

Figure 6. Treatment with auranofin leads to anti-NB activity *in vivo*.

(A) *MYCN*-amplified NB PDX and cell line xenograft models, COG-N-561, COG-N-452, COG-N-496 and IMR5, as well as the *MYCN*-wt cell line SK-N-SH xenografts, were randomized into treatment cohorts, as described in the Materials and Methods section. Auranofin was administered intraperitoneally, at a dosage of 10 mg/kg, six days a week (Monday-Saturday). Tumor measurements were performed every other day by calipers, and the average tumor volume + SEM for each cohort is displayed. **(B)** The ferroptosis markers transferrin receptor 1 (TfR1) and malondialdehyde (MDA) in non-treated and auranofin

treated IMR5 xenografts were detected by immunohistochemistry and their staining was quantified, error bars indicate +SEM. For figures 6A and 6B, Student's *t* test was performed, and p-values were corrected for multiple testing using Bonferroni method. Differences were considered statistically different if $p < 0.05$, * $p < 0.05$, ** $p < 0.01$, *** $p < 0.001$, **** $p < 0.0001$. **(C)** Graphical depiction of iron accumulation, ROS production and potential ferroptosis induction in *MYCN*-amplified NBs. Our model is that *MYCN*-amplified NBs have higher levels of intracellular iron, likely due to increased expression of the transferrin receptor 1 and lower expression of ferroportin. Iron can be lethal to the cell, if its levels are high, as it is also a major ROS producer. In order to counteract the potential oxidative stress, the MYCN overexpressing NBs express higher levels of the two subunits of system Xc-, SLC3A2 and SLC7A11, as well as GCLC, to provide the cell with cystine and establish an antioxidant protective system through glutathione production and GPX4 activation. Treating the *MYCN* NBs with selective inhibitors of the glutathione pathway results in elevated lipid peroxidation and finally ferroptotic cell death. Furthermore, inhibiting the parallel thioredoxin detoxification pathway with auranofin enhances sensitivity in the *MYCN* NBs (the illustration was created with BioRender.com).